Scientific paper

Synthesis, Characterization, and Theoretical Calculation of a Copper Complex of 3-Hydroxy-2-methylquinolin-4-carboxylate and 1,10-Phenanthroline

Yan-Hua Li, Xing-Jian Liu, Jian Huang, Yu Xie, Fei Deng, Xiu-Guang Yi^{1,2,3*}

¹ School of Chemistry and Chemical Engineering, Jinggangshan University, Ji'an 343009, PR China

² State Key Laboratory of High-Efficiency Utilization of Coal and Green Chemical Engineering, Yinchuan 750021, PR China

³ Jiangxi Hongjing Pharmaceutical Co., Ltd, Ji'an 343009, PR China

* Corresponding author: E-mail: 9920190013@jgsu.edu.cn and jayxgggchem@163.com

Received: 06-29-2025

Abstract

A copper complex containing mixed ligands [Cu(MCA)(Phen)· $3H_2O$)] (HMCA = 3-hydroxy-2-methylquinoline-4-carboxylic acid, Phen = 1,10-phenanthroline) was prepared by the hydrothermal method. Structure was characterized by single crystal X-ray diffraction. Solid state fluorescence photoluminescence measurement shows a strong emission peak at 620 nm, which is attributed to the characteristic electronic transitions and molecular stacking effects within the ligand. CIE color difference analysis indicates that the title complex exhibits red photoluminescence (chromaticity coordinates of 0.1256, 0.2418). In addition, solid-state UV-Vis diffuse reflectance experiments revealed that the titled complex has an energy band gap of 1.578 eV.

Keywords: Copper, crystal structure, photoluminescence, band gap.

1. Introduction

Metal organic frameworks (MOFs), as a novel coordination polymer, are formed through self-assembly of multidentate organic ligands (such as aromatic polyacids and polybasic bases) with transition metal ions. Their performance regulation is influenced by multiple factors such as the stability of the composite, ligand metal spacing, and intrinsic properties of the metal. Among ligands, organic carboxylic acids stand out due to their strong coordination ability, diverse coordination modes, and moderate balance between rigidity and flexibility. The coordination between the oxygen atom of carboxylic acid ligands and metal ions not only stabilizes the metal center, but also forms hydrogen bonds through deprotonation, thereby enhancing the structural integrity and stability of materials,² In addition, the multidentate nature of carboxylic acid ligands enables them to form chelating structures with multiple metal ions, further enhancing the stability of the complex.3 Nitrogen containing heterocyclic carboxylic acid ligands (such as quinoline carboxylic acid) can coordinate with metal ions through various ways such as monodentate, bidentate, or bridging, forming coordination polymers with different geometric configurations. For example, quinoline carboxylic acids can form 1D, 2D, and 3D structures through monodentate or bidentate coordination. ^{4,5} The rigid plane of the quinoline ring endows the complex with excellent structural stability, and the introduction of nitrogen-containing heterocyclic carboxylic acid ligands can significantly improve the thermal and mechanical stability of the coordination polymer. ^{6,7} The coordination between transition metals (such as Cu²⁺, Fe³⁺, etc.) and nitrogen-containing heterocyclic carboxylic acid ligands further enhances the functionality of the material. The synergistic effect of these metal ions with nitrogen atoms and carboxylic acid groups can form stable multi-core supramolecular structures. ⁸⁻¹⁰

Quinolinecarboxylic acid-based MOFs, due to their high porosity and tunable chemical structure, can efficiently adsorb pollutants in water, such as heavy metal ions (such as mercury, lead, cadmium, etc.), and have high selectivity and sensitivity. For example, certain MOFs can efficiently capture heavy metal ions and exhibit excellent selectivity through size exclusion, adsorption, and photo-

catalytic mechanisms.¹¹ In addition, fluorescence sensors based on MOFs have shown significant advantages in detecting heavy metal ions, such as sensitivity to mercury ions reaching ppb levels.¹² Quinolinecarboxylic acid-based MOFs have shown transformative potential in cutting-edge fields such as lithium battery energy storage, anti-cancer drug carriers, and solar energy conversion, fully demonstrating the core advantages of designability and functional diversity of metal organic complexes.^{13–17}

Based on this, we are interested in the crystal engineering of transition metal Cu²⁺ compounds containing 3-hydroxy-2-methylquinoline-4-carboxylic acid (HMCA) as ligand. ¹⁸ We report the solvothermal synthesis, X-ray crystal structure, photoluminescence and UV Vis diffuse reflectance spectral properties of a novel structural copper complex, and time-dependent density functional theory (TDDFT) calculations.

2. Experiment

2. 1. Experimental Materials and Instruments

All reagents and consumables used in the experiment are commercially available and can be used directly without purification. Infrared spectroscopy was measured using KBr tablets on a PE Spectrum One FT-IR instrument. Solid state UV-visible diffuse reflectance spectroscopy was performed using a computer-controlled TU1901 UV-visible spectrometer to measure diffuse reflectance. Fine ground powder samples are coated on BaSO₄ to achieve 100% reflectance. The photoluminescence performance was measured on the F97XP photoluminescence spectrometer.

2. 2. Synthesis of Title Complexes

Ligand HMCA (0.0304 g, 1.5 mmol), auxiliary ligand Phen (0.0099 g, 0.5 mmol), and $CuSO_4$ · $5H_2O$ (0.0125g, 0.5mmol) were added into a 25 mL stainless steel high-pressure vessel lined with polytetrafluoroethylene. Then, 10 mL of ethanol and 5 mL of water, and finally 0.15 mL of NaOH aqueous solution (1 mol/L) were added. The high-pressure reactor was heated to 120 °C in an oven and maintained for four days, then slowly cooled down to room temperature to obtain black block crystals, which are collected for single crystal X-ray diffraction testing. IR (KBr, cm $^{-1}$): 3434(s), 2925(w), 1633(w), 1586(m), 1520(w), 1436(m), 1396(w), 1339(w), 1237(w), 1174(w), 1147(w), 1112(w), 876(w), 846(w), 815(w), 776(w), 747(w), 721(w), 618(w).

2. 3. Collection and Refinement of Crystal Data for Title Complexes

A suitable single crystal (0.3 mm \times 0.2 mm \times 0.13 mm) was selected for measurement, and the structure of the complex was determined by X-ray single crystal dif-

fractometer (SuperNova charge coupled device) at room temperature of 293 K. The structure was analyzed using the ShelXT plugin in Olex2 software, and the structure was refined using the ShelXL plugin in Olex2 software. ^{19–22} All non-hydrogen atoms were refined anisotropically, while hydrogen atoms were refined using riding model. The crystallographic data of the title complex are presented in Table 1.

Table 1. The main crystallographic data of the title complex

Empirical formula	C ₂₃ H ₂₁ CuN ₃ O ₆
Formula weight	498.97
Temperature/K	293
Crystal system	triclinic
Space group	P-1
a/Å	6.9583(5)
b/Å	12.1607(8)
c/Å	12.7196(9)
α/°	77.027(6)
β/°	78.035(6)
γ/°	88.947(6)
V/Å ³	1025.60(13)
Z	2
$\rho_{\rm calc}/{\rm g~cm^{-3}}$	1.616
μ/mm ⁻¹	1.114
F(000)	514.0
Reflections collected	8185
Independent reflections (R_{int})	3759 (0.0197)
Data/restraints/parameters	3759/4/311
GOOF on F^2	1.036
R_1 , wR_2 $(I \ge 2\sigma(I))$	0.0571, 0.1404
R_1 , wR_2 (all data)	0.0711, 0.1519
$\Delta \rho_{\text{max}}$, $\Delta \rho_{\text{min}}$ / e Å ⁻³	1.60/-0.38

3. Results and Discussion

3. 1. Crystal Structure

Single crystal X-ray diffraction measurements show that the title complex belongs to the triclinic P-1 space group with a Z value of 2. Its unconformity unit is mainly composed of a neutral molecule composed of one Cu²⁺ ion, one MCA- ion, one Phen molecule, and three free water molecules. Cu2+ is four coordinated and the complex has a square-planar structure. The coordination sphere is composed of O1 and O2 of the HMCA and N2 and N3 of the auxiliary ligand Phen, as shown in Figure 1. The bond distances of Cu-O1, Cu-O2, Cu-N2, and Cu-N3 are 1.863(3), 1.892(3), 1.991(3), and 2.004(3) Å, respectively, as shown in Table 2. The C-H···O hydrogen bonding interaction enables the construction of a three-dimensional supramolecular skeleton; intramolecular hydrogen bonding: C8-H8... O3; C12-H12···O1; C23-H23···O2, intermolecular hydrogen bonds: O4-H4A···O3; O4-H4B···O5; O5-H5D···O6; O5-H5E···O2; O6-H6A···O4; O6-H6B···N1; C20-H20···

O4; C21–H21···O5), see Table 3 and Figure 2 for details. In addition to a large number of hydrogen bonds, this structure also shows abundant π ··· π stacking interactions (Cg1···Cg2; Cg1····Cg2; Cg2···Cg3; Cg3···Cg5), as shown in Table 4 and Figure 3, forming a three-dimensional supramolecular structure, as shown in Figure 4.

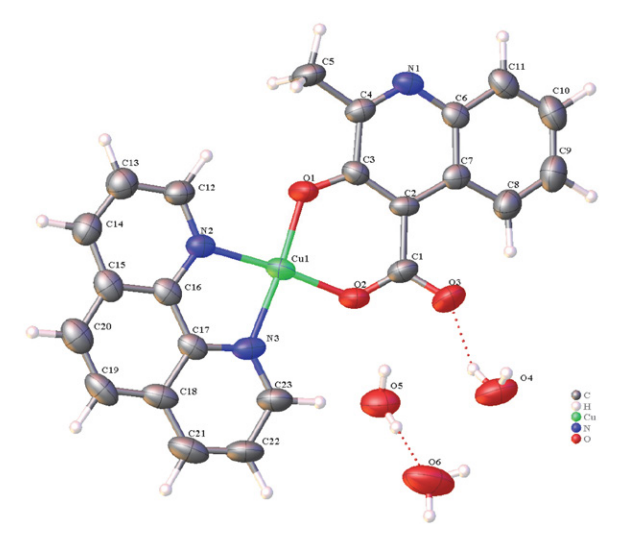


Figure 1. The molecular structure diagram of the title compound with 50% thermal ellipsoids.

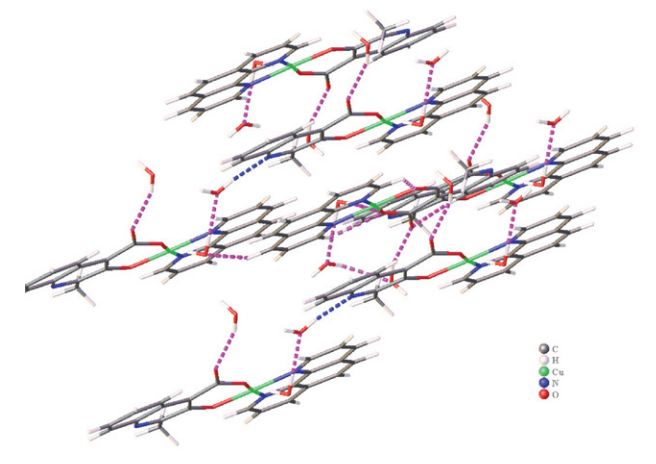


Figure 2. The hydrogen bonds diagram of the title compound (pink dotted line)

Table 2. The main bond lengths (Å) and bond angles (°) of the title complex

Bond	Distance [Å]	Bond	Distance [Å]
Cu-O1	1.869(3)	Cu-N2	1.994(3)
Cu-O2	1.891(3)	Cu-N3	2.004(3)
Angle	Angle [°]	Angle	Angle [°]
O1-Cu-O2	93.39(12)	C3-O1-Cu	126.7(3)
O1-Cu-N2	92.12(13)	C1-O2-Cu	128.8(3)
O1-Cu-N3	173.47(13)	C12-N2-Cu	127.4(3)
O2-Cu-N2	173.44(12)	C16-N2-Cu	112.5(3)
O2-Cu-N3	92.65(13)	C17-N3-Cu	111.9(3)
N2-Cu-N3	81.81(13)	C23-N3-Cu	130.0(3)

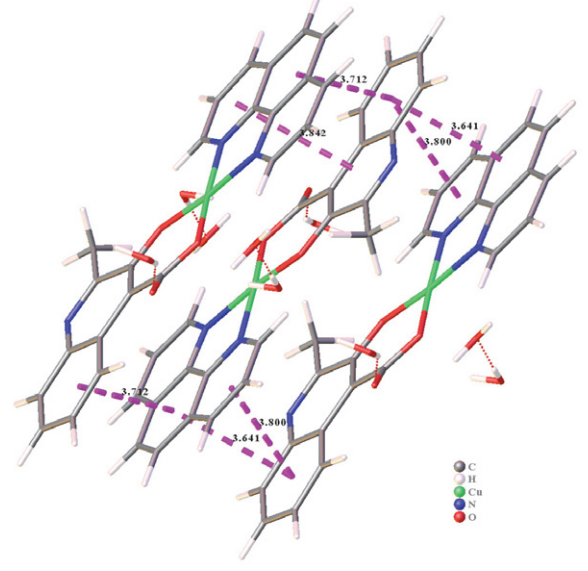


Figure 3. The $\pi \cdots \pi$ interaction diagram of the title complex (pink dotted line)

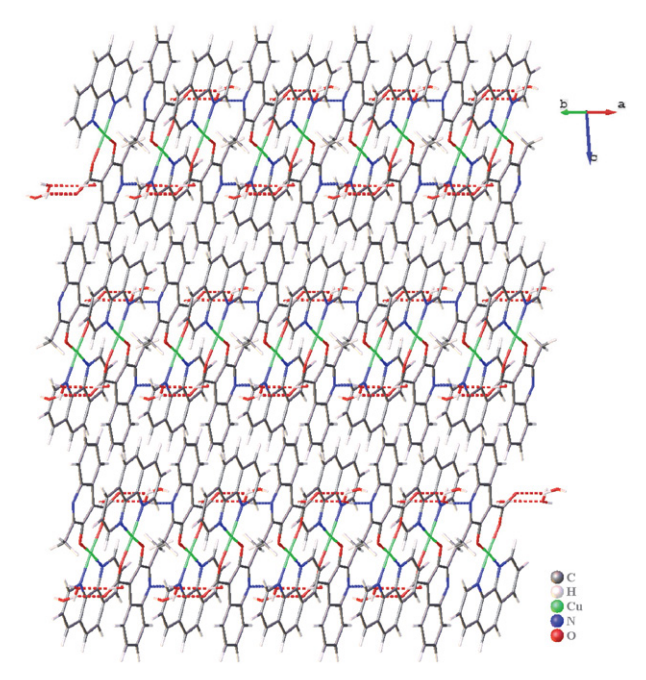


Figure 4. Stacking diagram

3. 2. Hirshfeld Surface Analysis

Hirshfeld surface analysis is an important tool for quantifying and visualizing weak intermolecular interactions in molecular crystals. By analyzing the size and shape of Hirshfeld surface, it can reflect the interactions between different atoms and the contact of molecules in the crystal. This analytical method can systematically characterize the weak interactions between molecules, reveal which parts of the molecules contribute mainly to the interactions, and the proportion of these interactions in the entire molecular crystal. ^{23–25} The weak intermolecular interactions were

Cg···Cg	Symmetry codes	Centroid-centroid distance (Å)	Slippage distance (Å)	Dihedral angle (Å)	
Cg1···Cg2	-x, $1 - y$, $1 - z$	3.712	1.725	5.506	
Cg1···Cg2	1 - x, $1 - y$, $1 - z$	3.641	0.994	5.506	
Cg1···Cg5	-x, $1 - y$, $1 - z$	3.568	1.056	2.131	
Cg2···Cg3	1 - x, $1 - y$, $1 - z$	3.800	1.485	5.989	
Cg3Cg5	-x, $1 - v$, $1 - z$	3.842	1.762	2.626	

Table 4. $\pi \cdot \cdot \cdot \pi$ stacking interactions of the title complex

Table 3. The main hydrogen bond lengths (Å) and bond angles (°) of the title complex

D-H···A	Symmetry codes	D-A (Å)	HA (Å)	DA (Å)	D-HA(°)
O4-H4A···O3	1+x,y,z	0.85	1.99	2.789(6)	157
O4-H4BO5	1 + x, y, z	0.85	2.23	2.997(6)	151
O5-H5DO6	1 + x, y, z	0.86(5)	1.96(5)	2.819(6)	176(8)
O5-H5EO2	1 + x, y, z	0.86(4)	2.26(5)	3.057(5)	153(5)
C6-H6A···O4	1 + x, y, z	0.85	2.38	2.882(7)	118
O6-H6B···N1	x, -1 + y, z	0.85	2.14	2.976(6)	169
C8-H8···O3	x, y, z	1.08	2.08	2.782(6)	120
C12-H12···O1	x, y, z	1.08	2.46	2.984(5)	109
C20-H20···O4	-1 + x, y, 1 + z	1.08	2.49	3.543(7)	163
C21-H21···O5	-x, -y, 1-z	1.08	2.58	3.330(6)	126
C23-H23···O2	x, y, z	1.08	2.57	3.075(6)	107

systematically characterized using the Crystal Explorer 3.1 program. The results showed that the $d_{\rm norm}$ shape index and curvature range of the complex were $-0.5727 \sim 1.3606$, $-0.9872 \sim 0.9963$, and $-3.7005 \sim 0.3254$, respectively, as shown in Figure 5.

The two-dimensional fingerprint image supplements the Hirshfeld surface and quantitatively summarizes the properties and types of intermolecular contacts experienced by molecules in the crystal.²⁶ The five main modes of action are H···H, C···C, C···H, O···H, and N···C, as shown in Figure 6. Among them, the H···H interaction shows a symmetrical distribution in the central region of the fingerprint spectrum, with a contribution rate of 46.3%, becoming the dominant mode of intermolecular interaction. Next are C···C, C···H, O···H, and N···C, with contribution rates of 13.5%, 7.5%, 5.9%, and 2.8%, respectively. C···H and O···H are common intramolecular hydrogen bonds,

distributed in a single wing shape in the two-dimensional fingerprint region.

3. 3. Solid-state Photoluminescence

At room temperature, photoluminescence measurements were conducted on the solid powder sample of the title complex, and the results are shown in Figure 7. From Figure 7, it can be clearly seen that the photoluminescence spectrum of the title complex exhibits effective energy absorption in the wavelength range of 525–675 nm. When excited at a wavelength of 397 nm, its emission spectrum shows a sharp band at 620 nm in the blue region. From this, it can be inferred that the title complex is a typical blue luminescent material. The emission band is located in the blue region, with CIE1931 chromaticity coordinates of (0.1256, 0.2418), as shown in Figure 8.

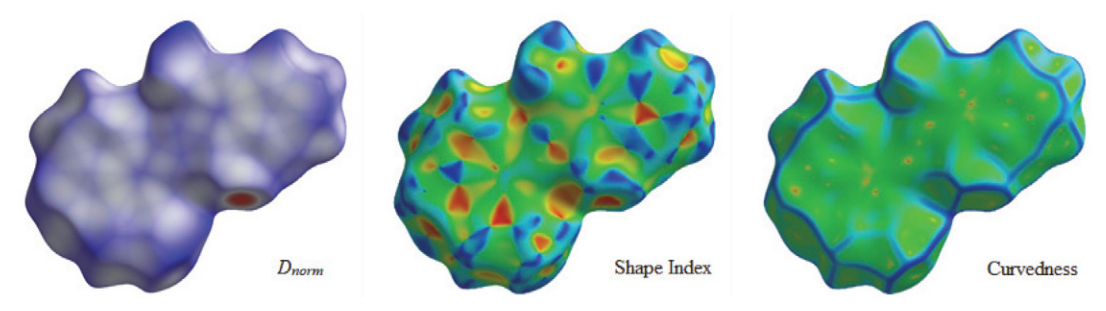


Figure 5. The Hirshfeld surface picture of the title complex

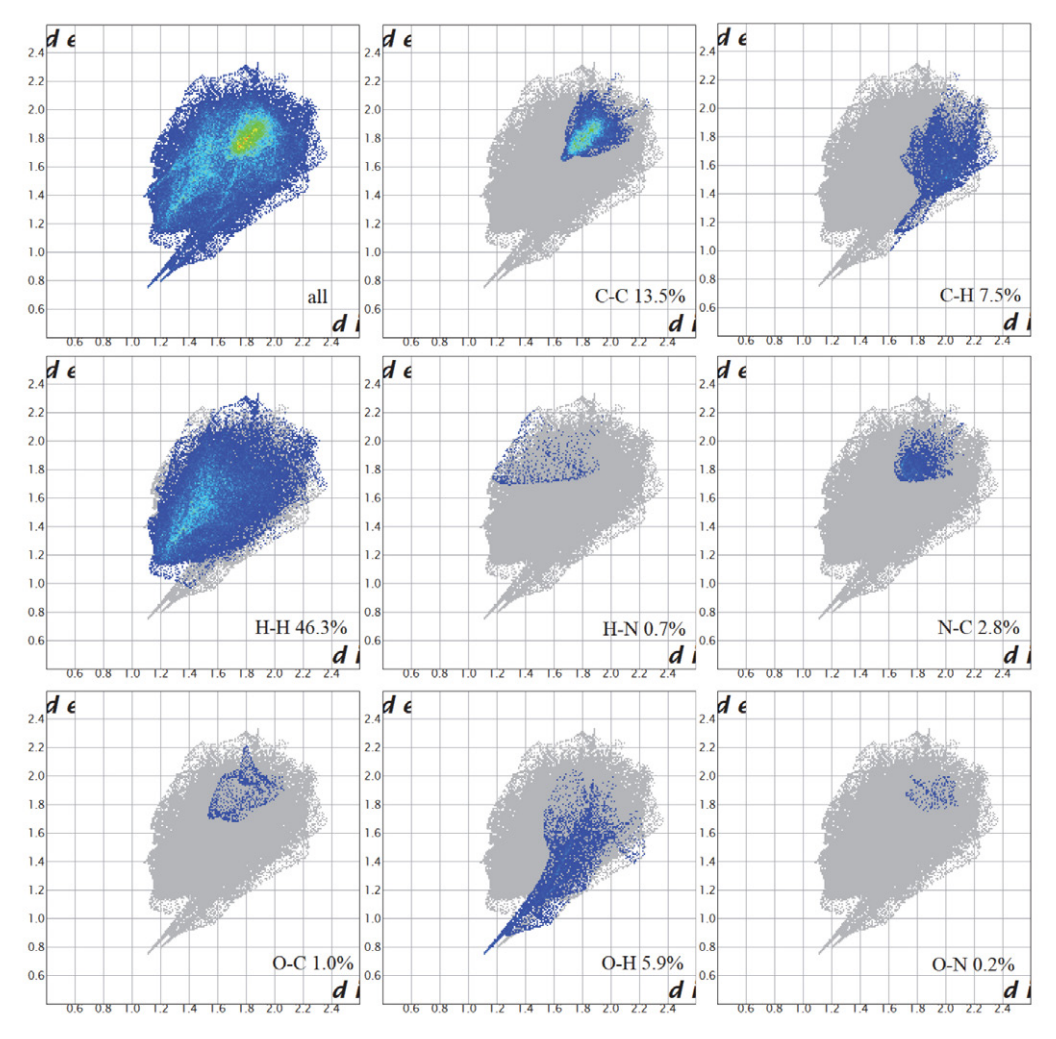


Figure 6. 2D fingerprint of the title complex (global 2D fingerprint and fingerprint of different molecular connections)

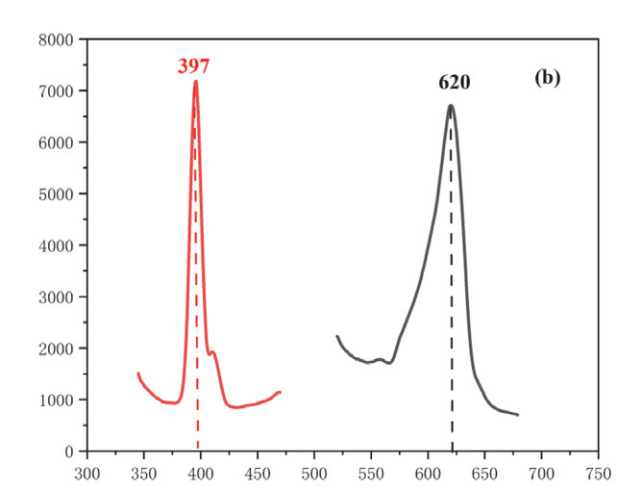


Figure 7. Solid state photoluminescence spectra of the title complex

3. 4. Solid State Diffuse Reflectance Spectroscopy (DRS)

In order to gain a deeper understanding of the conductivity of composites, solid-state UV Vis diffuse reflec-

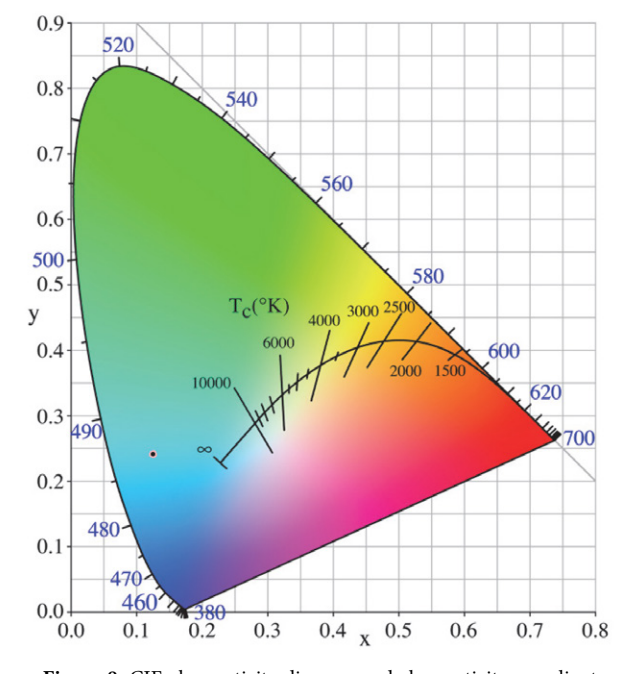


Figure 8. CIE chromaticity diagram and chromaticity coordinates of the emission spectrum of the title complex

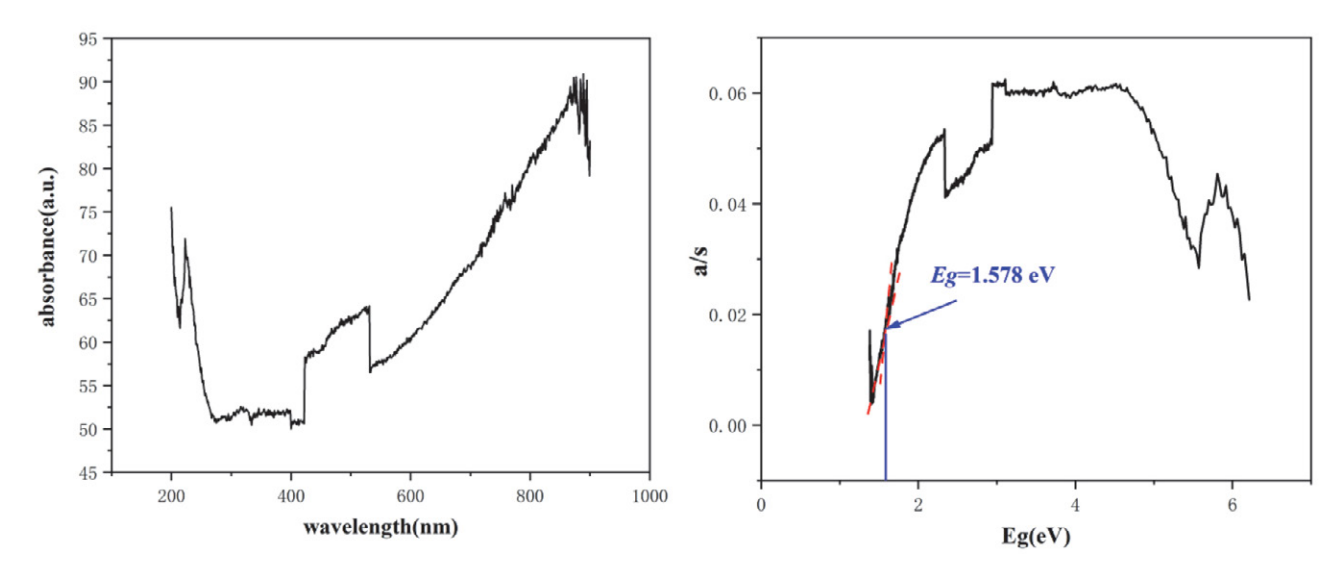


Figure 9. The UV-Vis spectra and the solid-state UV-Vis diffuse reflectance spectrum of the complex

tance technology has gradually become an important research tool. Under ultraviolet excitation, electrons in the complex absorb energy, transition from the ground state to the excited state, and exhibit absorption phenomena in the ultraviolet region. Through this process, relevant information about the conductivity of the material can be obtained.²⁷ Solid state samples of the title complex were measured by UV Vis DRS at room temperature using Ba₂SO₄ as the 100% reflective surface. The data processing is mainly based on the formulas proposed by Tauc, Davis, and Mott, commonly referred to as Tauc graphs.²⁸ The formula is $(ahv)^{1/n} = C(hv)^{1/n}$ $-E_{o}$), where a represents the absorbance index, h is Planck's constant, ν is frequency, C is constant, and E_g represents the semiconductor band gap width.^{29,30} The measurement results show that the title complex belongs to a narrow band gap semiconductor with an energy band gap of 1.578 eV, as shown in Figure 9.

3. 5. Theoretical Calculation

The HOMO and LUMO of the title complex (HO-

MO: highest occupied molecular orbital; LUMO: lowest unoccupied molecular orbital) are shown in Figure 10. HOMO is the highest energy level orbital occupied by electrons in a molecule, with strong electron donating ability, mainly related to the π bond structure of the ligand, and the electron density is highly concentrated on the π orbital of the ligand,³¹ The energy is -0.189668 a.u. In contrast, LUMO, as an electron acceptor, has lower energy and stronger electron acceptance ability, which is related to the π orbital of the ligand, and the electron density is concentrated on the aromatic ring or other π orbitals of the ligand. The energy is -0.123450 a.u. The energy difference between LUMO and HOMO is 0.066218 a.u., which is sufficient to allow charge transfer from HOMO to LUMO. Based on this observation, it is proposed that the photoluminescence of the title complex can be attributed to the charge transfer between ligands (LLCT: from the HOMO of the ligand HMCA π orbital to the LUMO of the ligand Phen π orbital). The calculation result is consistent with the experimental observation result.

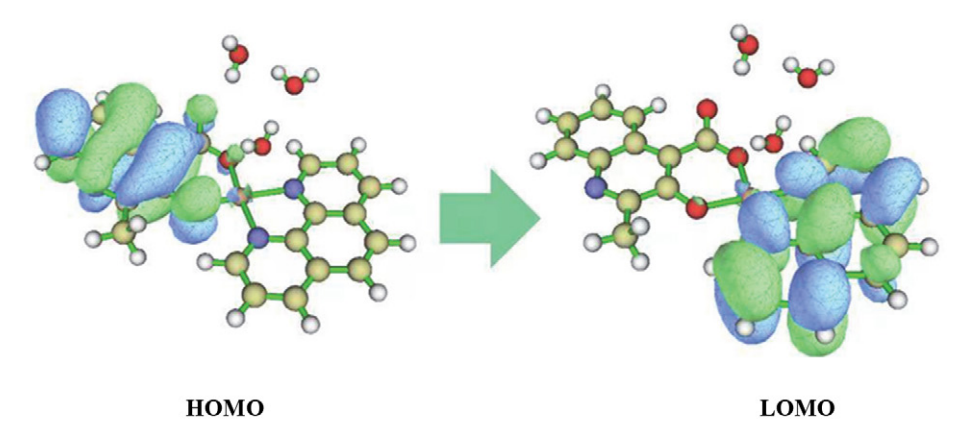


Figure 10. HOMO (left) and LUMO (right) of the complex

4. Conclusion

In summary, a novel Cu(II) mononuclear complex with excellent luminescent properties was successfully prepared by hydrothermal method, and its crystal structure was determined by single crystal X-ray diffraction. The structure is mainly constructed by hydrogen bonding and $\pi^{...}\pi$ interactions to form a three-dimensional supramolecular complex. The solid-state photoluminescence measurement results show that the complex exhibits a blue emission band at 620 nm, with CIE chromaticity coordinates of (0.1256, 0.2418). Solid state DRS measurements indicate that the complex is a high-performance semiconductor material with a band gap E_{σ} of 1.578 eV.

Supplementary Materials and Data Availability

Crystallographic data have been deposited with the Cambridge Crystallographic Data Center, CCDC 2468160. Copies of the data can be obtained free of charge from the Director, CCDC, 12 Union Road, Cambridge, CBZ, 1 EZ, UK; email: deposit@ccdc.cam.ac.uk or http://www.ccdc.cam.ac.uk.

Acknowledgements

The authors thank the National Natural Science Foundation of China (22168018), the National Natural Science Foundation of Jiangxi, China (20232BAB203048), the National Natural Science Foundation of Jiangxi Ji'an, China (20244-018539) and the Open Project of State Key Laboratory for Efficient Utilization of Coal and Green Chemical Industry (2025-KF07) for supporting this work.

Declaration of Competing Interest

The authors declare that they have no known competing financial interests or personal relationships that could have appeared to influence the work reported in this paper.

Data availability

Data will be made available on request.

5. References

- R. Wang, J. Gao, M. Vijayalakshmi, H. Tang, K. Chen, C. V. Reddy, R. R. Kakarla, P. M. Anjana, M. Rezakazemi, B. Cheolho, J. Shim, T. M. Aminabhavi, *Chem. Eng. J.* 2024, 496, 154294. DOI:10.1016/j.cej.2024.154294
- T. R. Cook, Y. R. Zheng, P. J. Stang, Chem. Rev. 2013, 113, 734–777. DOI:10.1021/cr3002824
- A. Byrne, N. J. English, U. Schwingenschlögl, D. F. Coker, J. Phys. Chem. C 2015, 120, 21–30.
 DOI:10.1021/acs.jpcc.5b08964
- C. B. Liu, Y. Cong, H. Y. Sun, Acta Crystallogr. Sect. E: Struct. Rep. 2012, 68, m1177. DOI:10.1107/S1600536812035209
- X. L. Li, G. Z. Liu, Z. Kristallogr. NCS. 2010, 225, 761–762.
 DOI:10.1524/ncrs.2010.0335

- H. H. Chen, R.Y. Kuang, Y. Wu, H. Y. Guo, S. H. Xie, D. H. Chen, X. G. Yi, *J. Chem. Crystallogr.* 2021, 51, 516-522.
 DOI:10.1007/s10870-020-00874-x
- X. X. Wang, J. J. Zhao, J. J. Zhang, N. Ren, S. K. Shi, *J. Therm. Anal. Calorim.* 2022, 147, 10337–10349.
 DOI:10.1007/s10973-022-11281-z
- M. Selvaganapathy, N. Raman, J. Chem. Biol. Ther. 2016, 1, 108. DOI:10.4172/2572-0406.1000108
- J. D. Rolfes, M. Van Gastel, F. Neese, *Inorg. Chem.* 2020, 59, 1556–1565. DOI:10.1021/acs.inorgchem.9b03474
- J. C. Ott, D. Bürgy, H. Guan, L. H. Gade, Acc. Chem. Res. 2022, 55, 857–868. DOI:10.1021/acs.accounts.1c00737
- S. Essalmi, S. Lotfi, A. BaQais, M. Saadi, M. Arab, H. A. Ahsaine, RSC Adv. 2024, 14, 9365–9390.
 DOI:10.1039/D3RA08815D
- P. Samanta, S. Let, W. Mandal, S. Dutta, S.K. Ghosh, *Inorg. Chem. Front.* 2020, *7*, 1801–1821.
 DOI:10.1039/D0QI00167H
- 13. N. Javed, T. Noor, N. Iqbal, S. R. Naqvi, *RSC Adv.* **2023**, *13*, 1137–1161. **DOI**:10.1039/D2RA06741B
- N. Singh, J. Kim, J. Kim, K. Lee, Z. Zunbul, I. Lee, E. Kim, S. G. Chi, J. S. Kim, *Bioact. Mater.* 2023, *21*, 358–380.
 DOI:10.1016/j.bioactmat.2022.08.016
- I. Tibbetts, G. E. Kostakis, *Molecules* 2020, 25, 1291.
 DOI:10.3390/molecules25061291
- Y. Xu, H. Xue, X. Li, X. Fan, P. Li, T. Zhang, K. Chang, T. Wang, J. He, *Nano Res. Energy* 2023, 2, e9120052.
 DOI:10.26599/NRE.2023.9120052
- O. Yildirim, M. Bonomo, N. Barbero, C. Atzori, B. Civalleri, F. Bonino, G. Viscardi, C. Barolo, *Energies* **2020**, *13*, 5602.
 DOI:10.3390/en13215602
- 18. X. G. Yi, X. N. Fang, J. Guo, J. Li, Z. P. Xie, *Acta Chim. Slov.* **2020**, *67*, 507–515. **DOI**:10.1107/S1600536812035209
- Y. Kenzhebayeva, I. Gorbunova, A. Dolgopolov, M. V. Dmitriev, T. S. Atabaev, E. A. Stepanidenko, A. S. Efimova, A. S. Novikov, S. Shipilovskikh, V. A. Milichko, *Adv. Photon. Res.* 2024, 5, 2300173. DOI:10.1002/adpr.202300173
- G. M. Sheldrick, *Acta Crystallogr. A* 2008, A64, 112–122.
 DOI:10.1107/S0108767307043930
- G. M. Sheldrick, Acta Crystallogr. C 2015, C71, 3–8.
 DOI:10.1107/S2053229614024218
- O. V. Dolomanov, L. J. Bourhis, R. J. Gildea, J. A. K. Howard, H. Puschmann, J. Appl. Crystallogr. 2009, 42, 339–341.
 DOI:10.1107/S0021889808042726
- S. L. Tan, M. M. Jotani, E. R. T. Tiekink, Acta Crystallogr. Sect. E. 2019, 75, 308–318. DOI:10.1107/S2056989019001129
- 24. S. Suda, A. Tateno, D. Nakane, T. Akitsu, Akitsu T. *J. Org. Chem.* **2023**, *13*, 57–85. **DOI:**10.4236/ijoc.2023.132006
- G.Shabir, H. Ghulam, A. Saeed, H. Tasawwar, T. Hökelek, M. F. Erben, U. Flörke, *J. Mol. Model.* 2021, 27, 296.
 DOI:10.1007/s00894-021-04910-1
- 26. D. F. Mertsalov, V. P. Zaytsev, K. M. Pokazeev, M. S. Grigoriev, A. V. Bachinsky, S. T. Çelikesir, M. Akkurt, S. Mlowe, *Acta Crystallogr. Sect. E* 2021, 77, 255–259. DOI:10.1107/S2056989021001481
 - TWO WEDDINGS OF THE TOTAL
- 27. X. G. Yi, F. P. Lai, Y. Y. Yan, C. Zhang, W. P. Li, J. Chem. Res.

- **2020**, 45, 295–304. **DOI:**10.1177/1747519820948363
- 28. T. Peng, X. Y. Chen, T. Q. Qiu, J. L. Fan, *Rev. Roum. Chim.* **2024**, *69*, 49–56. **DOI:**10.33224/rrch.2024.69.1-2.06
- W. Li, Q. Wang, F. Cui, G. Jiang, RSC Adv. 2022, 12, 17984– 17989. DOI:10.1039/D2RA02660K
- 30. J. Li, P. Tu, Q. Yang, *Sci. Rep.* **2024**, *14*, 10643. **DOI:**10.1038/s41598-024-60250-z
- K. E. Srikanth, A. Veeraiah, T. Pooventhiran, R. Thomas, K. A. Solomon, Ch. J. Soma Raju, J. N. L. Latha, *Heliyon* **2020**, *6*, e04106. **DOI**:10.1016/j.heliyon.2020.e04106

Povzetek

Bakrov kompleks $[Cu(MCA)(Phen)\cdot 3H_2O)]$ (HMCA = 3-hidroksi-2-metilkinolin-4-karboksilna kislina, Phen = 1,10-fenantrolin) smo pripravili s hidrotermalno metodo. Struktura je bila določena z monokristalno rentgensko difrakcijo. Meritve fluorescenčne fotoluminiscence v trdnem stanju kažejo močan emisijski vrh pri 620 nm, ki se pripisuje značilnim elektronskim prehodom in molekularnim učinkom zlaganja znotraj liganda. Analiza barvne razlike CIE kaže, da kompleks izkazuje rdečo fotoluminiscenco (kromatične koordinate 0,1256, 0,2418). Poleg tega so eksperimenti UV-Vis difuzne reflektance v trdnem stanju pokazali, da ima kompleks energijsko vrzel 1,578 eV.



Except when otherwise noted, articles in this journal are published under the terms and conditions of the Creative Commons Attribution 4.0 International License